Interaction of manzamine A with glycogen synthase kinase 3β: a molecular dynamics study

*D. I. Osolodkin,[a] D. A. Shulga,[b] V. A. Palyulin,[a,b] and N. S. Zefirov[a,b]**

[a]Department of Chemistry, M. V. Lomonosov Moscow State University. Build. 3, 1 Leninskie Gory, 119991 Moscow, Russian Federation. Fax: +7 (495) 939 0290. E-mail: zefirov@org.chem.msu.ru
[b]Institute of Physiologically Active Compounds, Russian Academy of Sciences. 1 Severnyj proezd, 142432 Chernogolovka, Moscow Region, Russian Federation. Fax: +7 (496) 524 95 08.

The search for the possible binding site of manzamine A to glycogen synthase kinase 3β(GSK-3β) was performed by molecular docking followed by molecular dynamics simulation and calculations of the Gibbs free energy of inhibitor—kinase binding. The cavity between the glycine-rich loop, the loop C, and the activation loop is the most likely site of interaction.

Key words: glycogen synthase kinase 3, manzamine A, molecular dynamics, docking, MM-PBSA method.

Human glycogen synthase kinase 3 (GSK-3) is a serine/threonine protein kinase discovered in the studies of glycogen metabolism.[1] Recently, it was established that the role of this enzyme is not reduced to phosphorylation of glycogen synthase; GSK-3 is involved in hyperphosphorylation of tau protein,[2] in the formation of amyloid plaques during Alzheimer´s disease,[3] and in phosphorylation of β-catenin (being complexed with axin and APC),[4] various gene transcription factors, and many other protein substrates.[5] In most cases, the GSK-3-mediated phosphorylation leads to inhibition of substrate activity.[5] GSK-3 was also found in parasites, such as causative agents of malaria *Plasmodium falciparum* and trypanosomiasis *Trypanosoma brucei*.[6,7]

There are two isoforms of GSK-3, *viz.*, GSK-3α (51 kDa) and GSK-3β (47 kDa), which are encoded by distinct genes.[8] Both isoforms are expressed in the brain; however, the expression level of the α-isoform in peripheral organs is higher than in the brain.[9] The GSK-3 isoforms play different roles in the organism.[10] In particular, only the α-isoform of GSK-3 is involved in the formation of amyloid plaques in the case of Alzheimer´s disease,[3] whereas the β-isoform mainly interacts with presenilin-1 and tau protein.[11] The identity of the amino acid sequences of the GSK-3 isoforms is 98% for the catalytic domain ("kinase domain"). The α-isoform differs from the β-isoform in an extended N-terminal glycine-rich tail.[8] The majority of competitive inhibitors of GSK-3 known to date are not selective between its isoforms.[12]

A salient feature of GSK-3 is preferred phosphorylation of substrates containing the (S/T)XXX[(S/T)P] amino acid sequence, where (S/T) is a serine or threonine residue, X is any amino acid residue, and [(S/T)P] is a prephosphorylated serine or threonine residue (usually, the phosphorylating agent is casein kinase II).[13] Tau protein can also be phosphorylated at non-primed sites, although the efficiency of this process is lower.[14] Recognition of the primed substrates is mediated by the interaction with the cluster of basic amino acid residues Arg96, Arg180, and Lys205 (from this point on, numeration of the residues is given according to the GSK-3β sequence unless otherwise stated).[15,16] This site also participates in the kinase autoinhibition upon phosphorylation of the regulatory residue Ser9 with protein kinase B (Akt/PKB).[15,17]

The structure of the catalytic domain of GSK-3β has been the subject of numerous X-ray studies. Twenty two structures of the kinase were available in the Protein Data Bank[18] as of October 2009, with different molecules occupying the ATP binding site, the axin binding site, the priming phosphate binding site, as well as differing in phosphorylation state of the regulatory Tyr216 residue. Significant structural differences appear only upon phosphorylation of this residue and lead to twofold increase in the kinase activity compared to the non-phosphorylated form. Namely, the side chain of Tyr216 is rotated by 120° and the phosphate group forms salt bridges with the Arg220 and Arg223 residues. Other differences between the structures correspond to small position fluctuations of the side chains and the backbone due to induced fit of the protein structure to the bound ligand.

GSK-3 inhibitors can be used for treatment of various diseases including type 2 diabetes,[19,10] Alzheimer´s dis-

Published in Russian in *Izvestiya Akademii Nauk. Seriya Khimicheskaya,* No. 10, pp. 1932—1943, October, 2010.

ease[2] and other neurodegenerative diseases,[10] mood disorders (bipolar disorder and unipolar depression),[19] various kidney diseases,[20] inflammatory processes,[19] prostate cancer,[21] mixed-lineage leukemia,[22] as well as disorders of sleep and circadian rhythm.[10] Most GSK-3 inhibitors known to date are ATP competitive and interact with the conservative ATP binding site[23]. Consequently, they are usually not very selective against other kinases. Non-competitive ATP inhibitors, which interact with other, less conservative regions of the enzyme structure, lack these drawbacks. Non-competitive GSK-3 inhibitors are mainly represented by two classes of compounds, *viz.*, synthetically accessible thiadiazolidinones (*e.g.*, TDZD-8, **1**)[24,25] and less studied, naturally occurring manzamines (*e.g.*, manzamine A, **2**) isolated from sponges.[26—28]

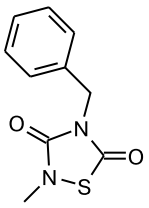

1

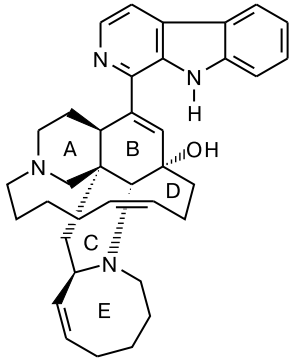

2

Manzamines are alkaloids containing the β-carboline fragment and a characteristic polycyclic framework. They are synthesized by *Micromonospora sp.* bacteria (strain M42)[29] and can be isolated from the sponges belonging to the geni *Haliclona*,[30] *Petrosiidae*,[29] *Pellina*, and some other.[31] Manzamine A exhibits antiviral (anti-HIV), antifungal, antibacterial,[32] and antimalarial[28] activity and is the best known representative of this class of compounds. Also, manzamine A inhibits human GSK-3 by the ATP non-competitive mechanism;[27] consequently, it may appear to be useful for the search or design of novel non-competitive inhibitors of the kinase. Rational search for such inhibitors requires detailed investigations of the interaction between manzamine A and GSK-3 that have not been performed so far.

In the present work, we analyze possible binding modes of manzamine A to GSK-3β. We performed a conformational analysis to rank the potential biologically active manzamine conformations, a search for potential binding sites by docking, and molecular dynamics (MD) simulation to identify the most probable mode of the interaction between manzamine A and GSK-3β.

Calculation Procedures

Molecular docking. Docking was performed using the AutoDock 4.01 program, which is based on the genetic algorithm of the optimal solution search.[33,34] The structure of the activated form of the kinase used in the docking experiments was retrieved from the PDB database[18] (access code 1GNG, see Ref. 16). Geometry optimization and preparation of the protein structure was done using the Sybyl 8.0 software suite.[35] The ligand and protein structures were prepared using the AutoDockTools 1.4.5 software.[36] The Gasteiger charges[37] were assigned to the protein and ligand atoms.

The potentials of the ligand-receptor interaction were calculated at the nodes of a grid surrounding all possible binding sites. Due to software limitations on the grid box size, three grids were constructed and 100 orientations of the ligand were generated for each grid box. The bond between the carboline moiety and polycyclic core of the ligand was explicitly marked as rotatable. The ligand orientations thus generated were clustered according to the root-mean-square deviation (RMSD) of non-hydrogen atoms between them; the threshold RMSD value was 2.0 Å. The representative structures from each cluster were used for further analysis.

Analysis of docking results. The binding energies for different ligand orientations were scored using the AutoDock scoring function[33] and the CScore package[38] (Sybyl 8.0) implementing the G_score,[39] D_score,[40] PMF,[41] and ChemScore[42] scoring functions. The choice of the ligand orientations for further studies was guided by the score values and visual pose analysis.

Molecular dynamics simulation was carried out using the AMBER 10 software suite.[43] In all cases, the AMBER ff99SB force field[44] was used for the protein molecule and the GAFF force field[45] was used for the ligand molecule. The partial atomic charges for the protein molecule were taken from the AMBER ff99SB library. The partial atomic charges for the ligand molecule were calculated following the AM1-BCC scheme[46] using the Antechamber 1.27 program.[47] The lengths of the bonds involving hydrogen atoms were constrained using the SHAKE algorithm[48] to speed up calculations. The net charge of the system was neutralized by adding a necessary number of chloride ions.

Periodic boundary conditions and an explicit representation of water molecules (TIP3P model[49]) were used during MD simulation. The box containing solvent molecules had the shape of a truncated octahedron. Water molecules were added automatically in such a manner that the minimum distance between the box boundary and the molecule being simulated was 8.0 Å. The number of water molecules added was 10515 for the *apo*-form of GSK-3β, 779 for free manzamine, 10462 for the manzamine—GSK-3β complexes formed in the sites **I** and **IV**, and 10433 and 10380 for the manzamine—GSK-3β complexes formed in the sites **II** and **III**, respectively. The temperature of the system was maintained at 300 K using the Langevin thermostat; the collision frequency parameter was 2 ps^{-1}. The following steps were performed during the preparation of the system to the productive dynamics simulations:

1) minimization of the energy of solvent molecules (500 steepest descent iterations and 500 conjugated gradient iterations) with force-field restraints imposed on positions of the ligand and protein atoms (500 kcal mol^{-1} $Å^{-2}$);

2) constant-volume gradual heating of the system from 0 to 300 K over a period of 50 ps (integration step 2 fs) using the force-field restraints imposed on positions of the ligand and protein atoms (2 kcal mol^{-1} $Å^{-2}$);

3) optimization of the density of the system over a period of 50 ps (integration step 2 fs) at constant pressure and temperature

using the force-field restraints on positions of the ligand and protein atoms (2 kcal mol^{-1} Å^{-2});

4) equilibration of the system over a period of 500 ps (integration step 2 fs) at constant pressure and temperature without force-field restraints.

MD simulation (integration step 2 fs) was carried out on 256 CPUs of the SKIF MSU "CHEBYSHEV" cluster at the Research Computing Center, Moscow State University. Ten nanoseconds were simulated. If the results obtained were ambiguous, additional simulation was performed.

Analysis of the results of MD simulation and conformational search. Visual analysis of the trajectories obtained from MD simulation was performed using the VMD molecular graphics program.[50] The correlation matrices were constructed using the ptraj program incorporated into the AMBER 10 suite. The elements of such a matrix are the correlation coefficients between the coordinates of C_α atoms in different amino acid residues along the trajectory. The correlation coefficient close to 1 corresponds to unidirectional motion, the correlation coefficient close to −1 corresponds to oppositely directed motion, while the nearly-zero correlation coefficient corresponds to uncorrelated motions of molecular fragments. The correlation maps based on the correlation matrices were constructed using the LabPlot 1.5.1 software.[51]

For better clarity of the results of conformational studies, the ligand trajectories were modified, *viz.*, the trajectory snapshots were aligned by the five carbon atoms comprising the most rigid fragment of the manzamine molecule (Fig. 1).

The binding energies were estimated using the MM-PBSA/GBSA method[52] implemented in the AMBER 10 package. It involves calculations of changes in the Gibbs free energy ΔG upon binding by evaluating the trajectory-average Gibbs free energy $\langle G \rangle$ for the ligand-protein complex (C), ligand (L), and free protein (P) structures:

$$\Delta\langle G \rangle = \langle G_C \rangle - \langle G_P \rangle - \langle G_L \rangle.$$

The Gibbs free energy was estimated from the relation

$$\langle G \rangle = \langle E_{MM} \rangle + \langle G_S \rangle - \langle TS_{MM} \rangle,$$

where E_{MM} is the molecular mechanics estimated energy of the structure and G_S is the Gibbs free energy of solvation calculated by numerically solving the Poisson—Boltzmann equation[53] (G_{S_PBSA}) or by the computationally simpler generalized Born technique[54] (G_{S_GBSA}). Normal mode analysis was used to calculate the entropy term TS_{MM}.[55]

In all cases, the binding energies were calculated by the three trajectories approach; the energy characteristics of free protein and ligand were estimated based on independent trajectories.

Identification of putative binding sites of manzamine A

The following criteria were used to choose 1GNG as a GSK-3β structure for docking. First, there is no ligand in the ATP binding site; this allows one to leave possible artifacts of crystallization of the ligand-protein complex out of consideration. Second, in this structure, the conformation of the phosphate binding site is fixed by the sulfate ion; this is a good approximation to the initial state of this site upon interaction with the substrate. Third, Tyr216 is phosphorylated in this structure, which corresponds to the activated state of the kinase. In addition, the fact that this structure of the kinase was used in the previous studies[28] enables a direct comparison of the results obtained.

Three hundred docking solutions falling into 107 different clusters were generated for the complex of GSK-3β with manzamine A. The cluster populations vary from one to dozens per cluster; however, low-populated clusters dominate. Typical representatives of clusters are shown in Fig. 2.

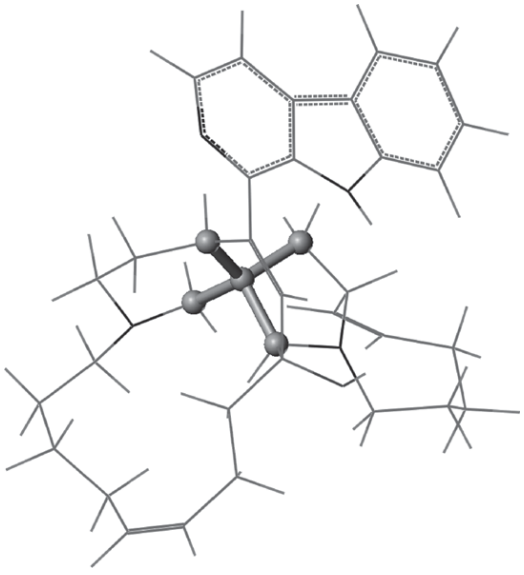

Fig. 1. A conformation of the manzamine A molecule corresponding to the global energy minimum. The fragment used for alignment is highlighted.

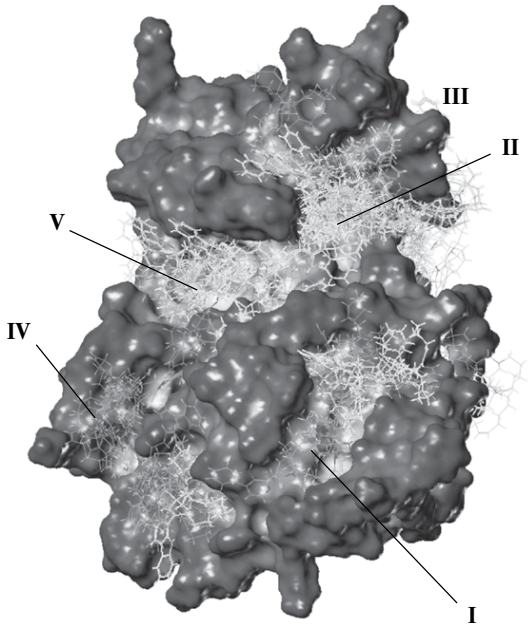

Fig. 2. Docking results. Shown are the representative structures of all possible clusters. The kinase surface is constructed using the Connolly algorithm.[56]

Five sites (**I**—**V**, see Fig. 2) for further analysis were identified on the surface of GSK-3β based on the docking results and published data. Interaction of the ligand with these sites may affect the functioning of the enzyme.

The axin[57] and FRAT [16] binding site (site **I**) mediates the formation of the complex of GSK-3β with axin that phosphorylates β-catenin, which plays an important role in the Wnt signalling pathway. The FRAT protein inhibits the formation of this complex, thus activating the pathway. Interactions with these proteins do not affect the catalytic activity of the kinase; however, the possible role of manzamine in this interaction was not studied so far. A study of the interaction of manzamine A with this site is interesting because it offers prospects for the design of inhibitors of the GSK-3β—axin interaction enabling selective regulation of the Wnt signalling pathway.

The cavity between the glycine-rich loop (residues 62—70), the loop C (residues 87—97), and the activation loop (residues 200—226) (site **II**) is formed by the key structural fragments involved in the activation of the kinase and in the kinase—substrate interaction.[58] This site is responsible for the recognition of the substrate priming phosphate group. Based on the docking results, a number of researchers believe that the TDZD inhibitors of GSK-3β (see Refs 24 and 59) interact with this site, which leads to violation of the interaction between the kinase and substrate.

Binding of manzamine A near the loop C (site **III**) was suggested[28] based on the results of a GOLD (see Ref. 39) docking study. The putative binding mode proposed in that study could not be exactly reproduced by us, but the key interaction, *viz.*, the hydrogen bond between the hydroxyl group of manzamine A and the backbone carbonyl oxygen of Arg92, was found. Such an orientation is usually scored quite low by both the AutoDock and CScore functions; nevertheless, we performed an MD simulation of this complex to test the hypotheses mentioned above.

Site **IV** is a possible binding site of allosteric inhibitors. By analogy with the published data,[60] one can assume that allosteric GSK-3 inhibitors interact with the amino acid residues Tyr140, Arg144, Arg220, Tyr221, Tyr222, and Pro255 and thus violate the interaction between the kinase and substrate. The possibility for such an interaction involving GSK-3 was not studied in detail so far.

The ATP binding site (**V**). Manzamine A should not interact with this site due to non-competitive character of its inhibitory activity.[27] Nevertheless, the docking program places the ligand to this site because it is sufficiently large and hydrophobic. Site **V** is usually ranked high by the scoring functions first of all due to a large surface area of contacts between the kinase and the ligand. We have not studied site **V** by the MD method.

The sites **I**, **II**, **IV**, and **V** are ranked high by all scoring functions used in the present work. Other ligand orientations generated by docking are ranked much lower and do not correspond to any experimental data available at the moment. No hypotheses on the mechanism of non-competitive inhibition may be proposed based on these alternative low-ranked solutions.

Conformational analysis of the manzamine A molecule

The manzamine A molecule comprises a complex polycyclic framework linked to an aromatic fragment. It seemed important to analyze the conformational behavior of this molecule in order to establish the extent to which the molecular conformation in the crystal[29] matches the solution conformation and that of the complexes with kinase. In addition, it was interesting to study the possibility of changes in the ligand conformation due to the interaction with the protein.

Conformational behavior of the ligand in complexes. To study the behavior of the bound manzamine, we extracted its coordinates from the MD trajectories I—IV corresponding to the sites **I**—**IV** (see above). The coordinates were aligned over the fragment including five carbon atoms comprising the base of the rigid framework of the ligand molecule (see Fig. 1). Visual monitoring of the trajectories thus prepared for each starting point made it possible to reveal a number of salient features. In all trajectories studied, the conformations of all rings in the aliphatic framework show no qualitative changes throughout the time interval of simulation. The most important conformational differences may consist in numerical values of the angle of rotation of the carboline fragment relative to the macrocyclic fragment and the torsion angle characterizing rotation of the C—O bond and the presence or absence of the intramolecular hydrogen bond O—H...N. Since the numerical values of these torsion angles could vary in arbitrary manner in the course of the molecular docking procedure, mention should be made of the possibility of formation of various conformations upon changes in these torsion angles. In this connection, one should also assess the probability of conformational transitions at room temperature in aqueous solution.

The parameters described above were used for characterization of specific features of the conformational behavior for each trajectory corresponding to a particular site. In the site **I**, the carboline fragment is rotated toward the hydroxyl group of the molecule and the intramolecular hydrogen bond is rather stable along the whole trajectory. This conformation corresponds to a global minimum of the ligand energy. In the case of trajectory II, the carboline fragment is also rotated toward the hydroxyl group. A distinctive feature of this trajectory is high lability of the intramolecular hydrogen bond (often, up to its frequent breakdown). The sites **III** and **IV** are characterized by the

flip of the carboline moiety "outward" from the hydroxyl group and by the stable intramolecular hydrogen bond despite the fact that in the starting conformations of the docked ligand the hydroxyl group is rotated "away" from the corresponding nitrogen atom (acceptor of the hydrogen bond). The energies of the conformations with the flipped carboline moiety is 1.4 kcal mol^{-1} higher than the energy of the global minimum .

Ligand behavior in aqueous solution. We also studied the behavior of the free ligand by the MD method to compare the results obtained with the ligand behavior in complexes. The starting point was an optimized conformation, the closest to the manzamine A conformation in the crystal. In the latter, the carboline fragment is oriented toward the hydroxyl group and there is the intramolecular hydrogen bond. The coordinates of manzamine atoms were extracted from the trajectory and processed analogously to the coordinates extracted from the trajectories of complexes (*vide supra*).

The motion of the free ligand in aqueous solution is similar to that mentioned above in the analysis of trajectory I. It is noteworthy that no flip of the carboline moiety by 180° was observed during the 10-ns simulation. This can be explained by both a rather high energy barrier to such a rearrangement and long characteristic times of this motion, which involves a concerted displacement of many atoms in the molecule. In addition, the ligand conformations in which the torsion angle of the carboline fragment is 0 and 180° are not energetically favorable. This fragment spends much time being rotated by ±30° relative to those values.

Molecular dynamics simulation of the complexes

The dynamics of four structures of the complexes corresponding to the sites **I**—**IV** as well as the *apo*-form of GSK-3β were studied by the MD method. The choice of the starting structures was guided by the CScore consensus scoring, *viz.*, the orientations scored the highest by the four scoring functions implemented in this software package were selected for the MD simulation. These structures are shown in Fig. 3.

MD trajectories 10 to 20 ns long (see below) were generated in the course of the simulation. The structures of the complexes were sufficiently stable along the trajectory, namely, the RMSD of the protein backbone atoms was at most 2.5 Å (see Fig. 4). This suggests their applicability for the ligand binding analysis. Small RMSD deviations are due to the thermal concerted motions of the kinase lobes relative to each other (so-called "chewing motions").

The trajectory of the *apo*-form of GSK-3β. The structure of the *apo*-form of GSK-3β changes only slightly during the MD simulation. Almost no large-scale motions of the kinase lobes relative to each other were revealed and

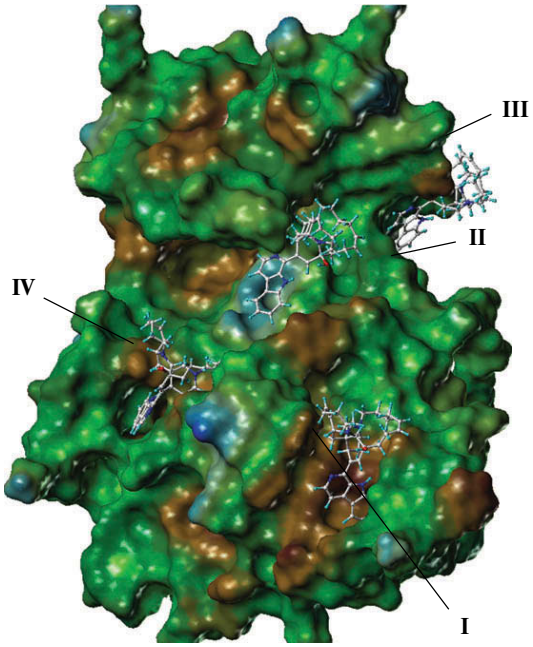

Fig. 3. The structures of complexes chosen for the MD simulation.*

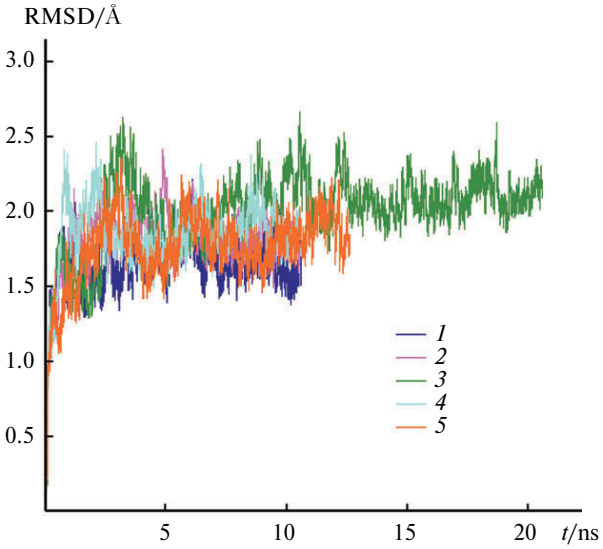

Fig. 4. The RMSD of the backbone atoms plotted *vs.* time in the MD simulation for the *apo*-form of GSK-3β (*1*) and for the sites **I** (*2*), **II** (*3*), **III** (*4*), and **IV** (*5*).

the loops also show only small-scale motions. The residues Arg96, Arg145, and Lys205 forming the priming phosphate binding site are relatively close to one another over the whole trajectory. The residue Glu211 occasionally forms a salt bridge with Lys205 rather than Arg96 (*cf.* other

* Figures 3, 4, and 9 are available in full color in the on-line version of the journal (http://springerlink.com).

trajectories); as a result, the activation loop does not approach the loop C. There is a hydrogen bond between the amino acid residues Gln89 and Asn95 responsible for the substrate recognition.[61] The results obtained suggest that the priming phosphate site is rather stable and accessible to the substrate even in the lack of negatively charged ions stabilizing it. The action of any factor destabilizing this site may lead to changes in the catalytic activity of the kinase.

The stability of the glycine-rich loop of the kinase, in particular, the Phe67 residue, is important. This loop plays the key role in the kinase—ATP binding and in the preparation of phosphate group transfer from ATP to the substrate.[58] Our simulation revealed small-scale thermal motions of this loop; however, its equilibrium conformation is quite stable and does not impede ATP binding.

The trajectory of the *apo*-form of GSK-3β obtained from the MD simulations was used as a reference for comparison with the trajectories I—IV of the proposed structures of the manzamine A—GSK-3β complexes.

Trajectory I. The structure of the complex rapidly stabilizes (it takes less than 0.5 ns) and remains almost unchanged throughout the simulation period (Fig. 5, *a*). The average structure of the complex is similar to the initial structure (Fig. 5, *b*) and differs from it by a noticeable (~60°) rotation about the bond between the carboline and polycyclic fragments of the ligand (Fig. 5, *c*). The carboline fragment goes inside the hydrophobic pocket (Fig. 5, *d*). The hydroxyl group of Tyr288 can form hydrogen bonds with the pyrrole hydrogen atom or with the hydroxyl group of the ligand; however, these bonds are not very stable, *viz.*, the occupancy of the hydrogen bond with the pyrrole atom is only 11%, whereas the hydrogen bond with the hydroxyl group of the ligand is formed from time to time. The hydroxyl group of the ligand is involved in the intramolecular hydrogen bond throughout the whole period of simulation.

It is important that the ligand binding indirectly affects the conformation of the activation loop owing to the interaction with Phe229. As a consequence, a strong salt bridge is formed between the residues Arg96 and Glu211 and the loop C moves toward the activation loop in the course of MD simulation. The volume of the substrate binding site is thus reduced, which may mediate noncompetitive inhibition of GSK-3β.

Trajectory II. The ligand rapidly (in less than 1 ns) moves to the region between the glycine-rich loop and the loop C. However, the orientation of the ligand is not very stable (Fig. 6, *a*) because there exist a number of distinct

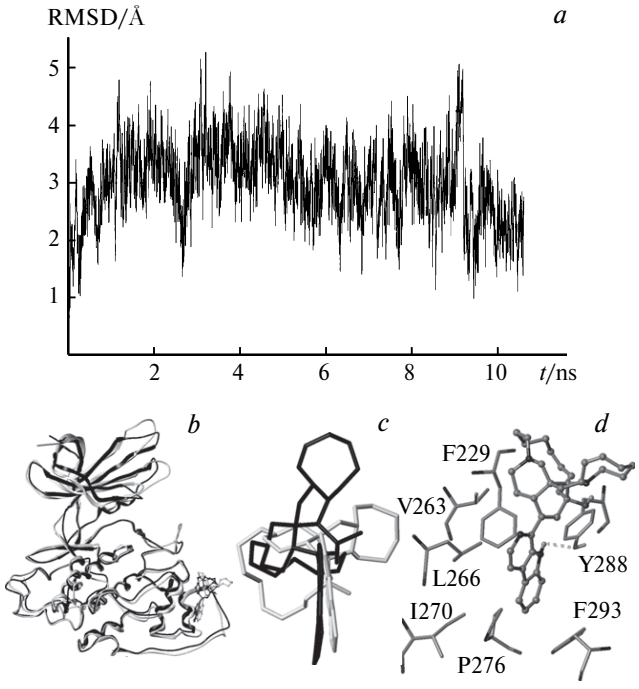

Fig. 5. Results of the MD simulation for the site **I**: the RMSD of the ligand atoms plotted *vs.* time of simulation (*a*); the overview of the average structure of the complex compared to the initial structure (*b*); here and in Figs 6 and 8 the initial structure is given in black and the average structure is given in light-grey; superimposition of the initial (black) and average (light-grey) structures of the ligand (*c*); and the binding mode of the ligand to the protein (*d*). Possible hydrogen bond is shown by dashed lines.

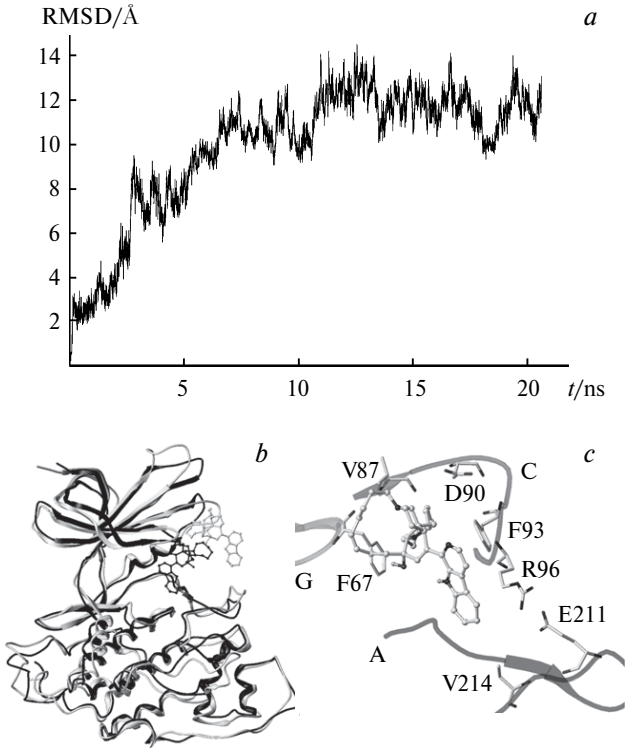

Fig. 6. Results of the MD simulation for the site **II**: the RMSD of ligand atoms plotted *vs.* time of the MD simulation (*a*); a comparison of the overview of the average structure of the complex and the initial strucure (*b*), and the binding mode of the ligand to the protein (*c*). The glycine-rich loop, the loop C, and the activation loop are denoted by "G", "C", and "A", respectively.

characteristic conformations with, *e.g.*, significantly different orientations of the carboline moiety. The MD simulation was extended to an additional 10 ns to collect more data, but the character of the ligand motion remained the same. Further analysis was performed for the 20-ns trajectory. It was found that the polycyclic core of the manzamine molecule is fixed between the glycine-rich loop and the loop C and moves together with the small kinase lobe (Fig. 6, *b*). The residues Val87, Asp90, Arg92, and Phe93 (loop C) form hydrophobic contacts with the rings C and E, while the residues Leu88 (loop C) and Phe67 (glycine-rich loop) form hydrophobic contacts with the rings D and E of manzamine A (Fig. 6, *c*). The hydrogen bond between Gln89 and Asn95 breaks down and the side chain of Gln89 reorients outward. The carboline fragment of manzamine A interacts with the activation loop (residue Val214) only when the kinase lobes approach each other. Owing to the binding to the ligand, the loop C moves toward the activation loop, thus gripping the priming phosphate binding site. This leads to the formation of a strong salt bridge between the amino acid residues Arg96 and Glu211. Thus, the presence of the manzamine molecule in the site **II** makes recognition of the phosphate group difficult. The interaction between the residues Phe67 and Leu88 plays an important role in the orientation of the glycine-rich loop for optimal interaction with ATP (see Ref. 61). The manzamine molecule also causes changes in the character of this interaction, while the breakdown of the hydrogen bond Gln89...Asn95 makes recognition of the substrate impossible;[61] consequently, this structure of the complex corresponds to a possible mechanism of non-competitive inhibition of the kinase.

Trajectory III. The surface area of the ligand—protein contact in the site **III** is relatively small; as a consequence, the ligand molecule moves across the surface of the kinase in the course of the MD simulation. The RMSD from the starting structure increases along the trajectory (Fig. 7, *a*) to more than 20 Å. The hydrogen bond between the ligand and the protein is replaced by an intramolecular hydrogen bond in the manzamine molecule that is characteristic of all other complexes. During the first 2 ns of simulation, the carboline fragment of the ligand interacts with the activation loop in the space between the lobes at the side opposite to the ATP binding site (RMSD about 10 Å) and causes the kinase lobes to move apart. However, this ligand orientation is unstable and manzamine continues its translational motion across the surface of GSK-3β. A relatively stable orientation is formed at 8 ns (Fig. 7, *b*). The hydroxyl group of the manzamine molecule is oriented toward the solvent molecule. There are almost no noticeable structural rearrangements in the priming phosphate binding site and the activation loop and the loop C do not approach each other; these facts do not allow one to formulate a reasonable explanation for the non-competitive inhibition mechanism through binding in this site.

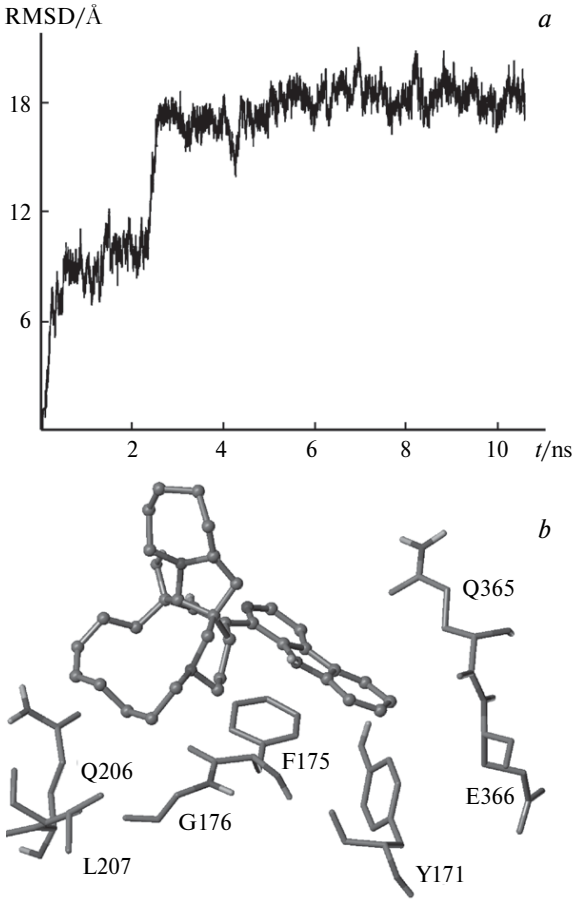

Fig. 7. Results of the MD simulations for the site **III**: the RMSD of ligand atoms plotted *vs.* time of the MD simulations (*a*) and the binding mode of the ligand to the protein in the equilibrium portion of trajectory (8—10 ns) (*b*).

Trajectory IV. Similarly to site **I**, the site **IV** is characterized by fast stabilization of the structure of the complex (Fig. 8, *a*). The average structure of the complex (Fig. 8, *b*) differs from the initial structure only in a small (less than 1 Å) displacement of the manzamine molecule toward the ATP binding site. The ligand orientation remains unchanged over a period of 8 ns; then, the molecule rapidly rotates in such a manner that the carboline fragment is oriented outward and the ligand contacts the protein molecule at the rings D and E and then only at the ring E, thus making the ATP binding site inaccessible. These changes can be due to a thermal fluctuation of the structure leading to the overcoming of the corresponding energy barrier. To refine the characteristics of the ligand orientation thus obtained, we performed an additional 2-ns MD simulation; however, no global changes in the structure of the complex were obtained. Note also that the activation loop and the loop C do not approach each other; this does not allow one to relate the mechanism of non-competitive inhibition to infringement of the phosphate binding. Nevertheless, infringement of the binding to the other sub-

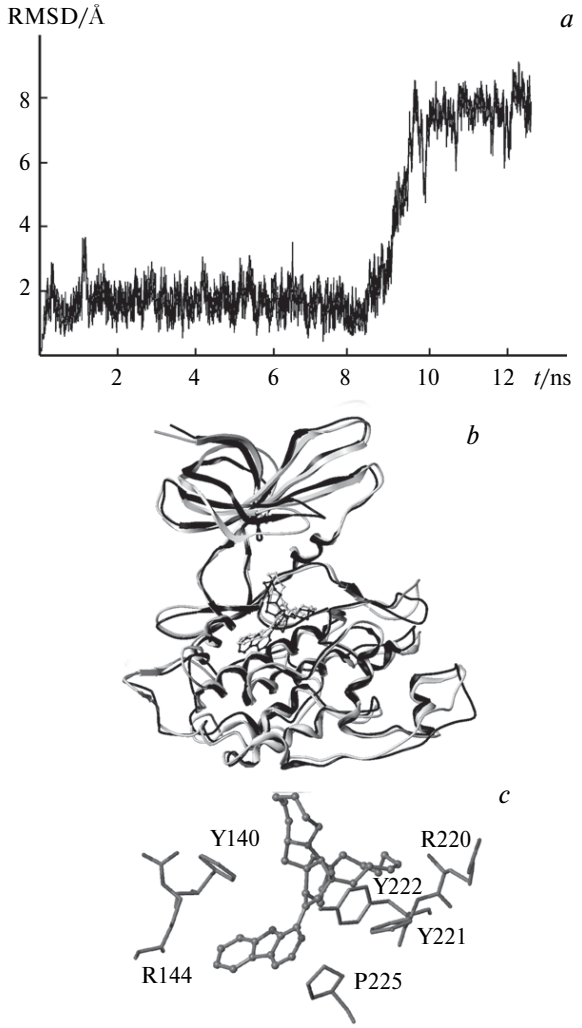

Fig. 8. Results of the MD simulation for the site **IV**: the RMSD of ligand atoms plotted *vs.* time of the MD simulations (*a*), a comparison of overview of the average structure of the complex and the initial strucure (*b*), and the binding mode of the ligand to the protein (*c*). The hydroxyl group of the ligand and the ring E of manzamine are oriented toward the solvent. Hydrogen atoms are not shown.

strate sites is possible; this binding is necessary for correct orientation of the phosphorylation site near the ATP molecule. A more detailed investigation of this hypothetical mechanism requires additional experimental data.

A relatively long period (8 ns) of stability of the initial structure allows this site to be treated as a site of possible non-competitive binding of inhibitors. The final structure of the complex is formed at 9 ns and agrees with the mechanism of ATP-competitive inhibition, thus going beyond the scope of this study.

Analysis of the correlation maps

A comparison of the correlation maps is a widely used method of analysis of MD trajectories. It allows one to reveal differences between concerted motions of large atomic groups, in particular, domains or structural fragments. The correlation maps were constructed for the equilibrium portions (see above) of all trajectories (Fig. 9).

Changes in the character of the motion in the vicinity of the amino acid residues 106—116 (helix C) and 320—330 in the presence of the inhibitor are clearly seen when comparing the correlation maps for the *apo*-form and the site **I** (see Fig. 9, *a*, *b*). Rather long distances between these amino acid residues and the inhibitor binding site can be explained by the allosteric effect of the inhibitor binding on the dynamic behavior of the protein molecule.

The correlation map for the trajectory II (see Fig. 9, *c*) was constructed using a portion corresponding to a 10—18 ns interval in the MD trajectory and characterized by a stable ligand orientation in the binding site between the glycine-rich loop and the loop C. If a molecule is placed in the site **II**, the most pronounced differences from the *apo*-form appear near the amino acid residues 250—260, which interact with the phosphate group of pTyr216. Thus, the binding of the ligand changes the character of motion of the activation loop; this can be an important factor in the mechanism of non-competitive inhibition of the kinase. In this case, the changes in the correlation map are most pronounced, although confined within a few amino acid residues.

The correlation map constructed for trajectory III (see Fig. 9, *d*) shows the least spread of data points compared to the other maps; this suggests no rigid domains in the protein structure. The complex for the site **III** is softer than the complex for the *apo*-form. However, the correlation maps show no fundamental differences and suggest that the kinase—manzamine binding has little effect on the character of protein motions. Higher plasticity of the protein compared to the *apo*-form can also be a consequence of analysis of a smaller portion of the MD trajectory.

Contrary to this, for the site **IV** (see Fig. 9, *e*) the protein becomes less "granular", *viz.*, the correlated and anti-correlated regions enlarge and the small and the large kinase lobes move in opposite directions. Similar motions were observed in the MD simulation of a complex of protein kinase A (PKA) with ATP (see Ref. 62). In addition, the character of motions near the activation loop (amino acid residues 205—220) noticeably changes; this may correspond to non-competitive inhibition.

Thus, our analysis of the correlation maps suggests that for all possible sites, except for the site **III**, local changes are induced compared to the map of the *apo*-form of GSK-3β. These changes can correspond to allosteric processes related to the kinase inhibition.

Estimation of binding energy

The binding energies were estimated by the MM-PBSA/GBSA method (3 trajectories) using the fol-

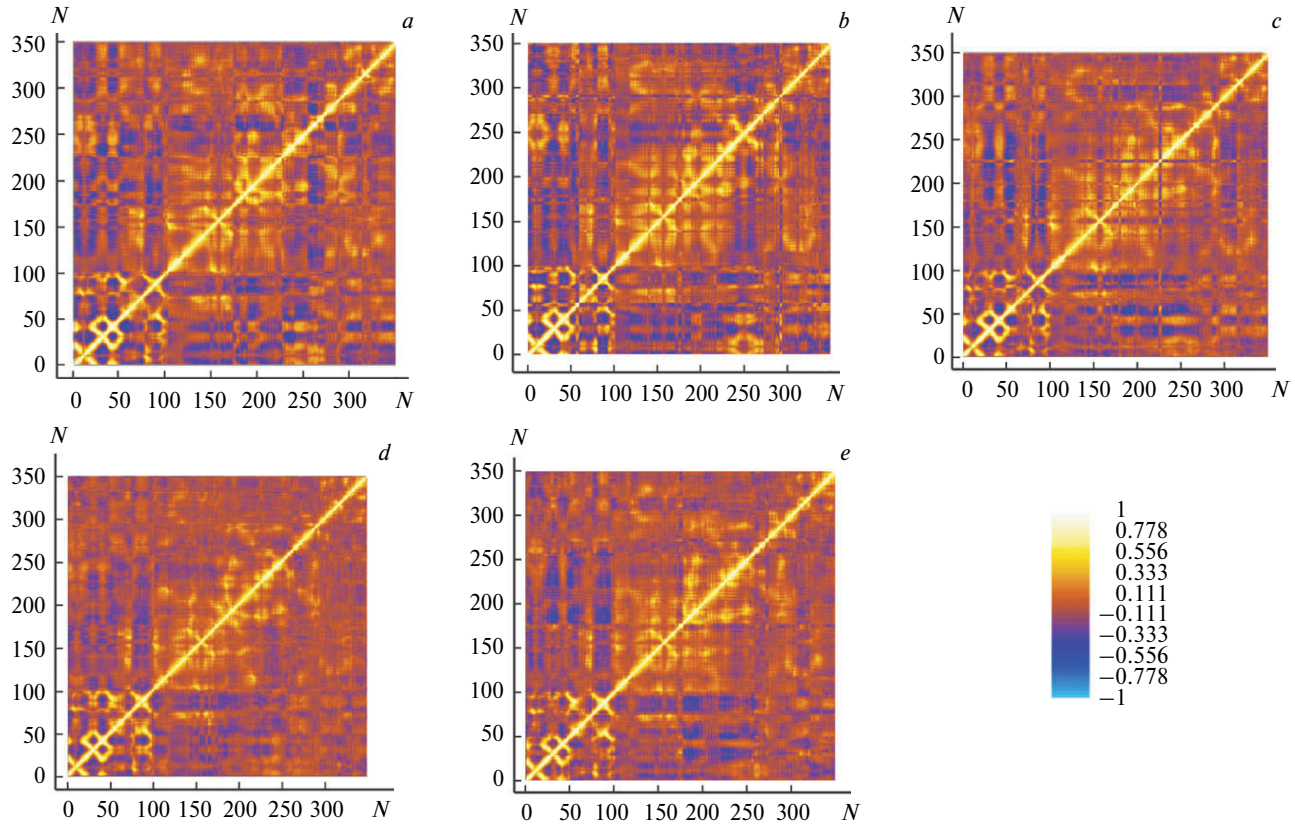

Fig. 9. Correlation maps of the MD trajectories: the MD trajectory for the *apo*-form of GSK-3β (*a*) and the MD trajectories I (*b*); II (*c*); III (*d*); and IV (*e*). The brightest regions correspond to high positive correlation, brown regions correspond to a nearly zero correlation, and blue regions correspond to negative correlation. *N* is the number of the amino acid residue in the amino acid sequence of GSK-3β.

lowing portions of trajectories: 1—10 ns for trajectory I; 10—18 ns for trajectory II; 8—10 ns for trajectory III; and 1—8 ns for trajectory IV. The calculated thermodynamic parameters are given in Table 1. Owing to large (in absolute value) ΔG values, a direct interpretation of the calculated binding free energies in terms of statistical thermodynamics, in particular, calculations of the binding constant, have no physical meaning. In other words, a comparison of this estimate with the experimental binding energy is senseless. However, the calculated binding energy values can be compared to one another.

Table 1 lists the relative binding energies to the sites **I**—**IV**. The Gibbs energy of binding to site **III** was chosen as a reference. For the site **II**, the Gibbs energy of binding is higher, whereas for the sites **I** and **IV** it is much higher than that calculated for the site **III**. The reason for such large differences is the difference in the surface areas of the ligand—protein contacts, because the manzamine binding mainly occurs through hydrophobic interactions and π—π-interactions with GSK-3. Thus, in this case the MM-PBSA/GBSA method is hardly applicable for the search for a binding site of an allosteric modulator to the protein. The energetically optimal binding mode may not be related to the inhibition mechanism. Meanwhile, this method gives the best results when comparing the binding constants of structurally similar ligands for the same active site.

Table 1. Calculated Gibbs free energies of manzamine A binding to the sites **I**—**IV** of GSK-3β

Region	$-\Delta E_{MM}$	$-\Delta G_{S\_PBSA}$	$-\Delta G_{S\_GBSA}$	$-T\Delta S$	$-\Delta G_{PBSA}$	$-\Delta G_{GBSA}$	$\Delta\Delta G_{PBSA}$	$\Delta\Delta G_{GBSA}$
I	112	30	19	17	125	113	143	154
II	157	23	3	12	168	149	100	118
III	208	75	74	15	268	267	0	0
IV	73	41	60	4	109	129	159	138

The ranking of sites

Since at present all MD methods provide no comprehensive answer to the inhibition mechanism, to improve the predictive power, it is appropriate to use several different techniques. Potential sites were ranked based on the results obtained by three methods of analysis of the MD trajectories, *viz.*, conformational analysis of the ligand, visual analysis of the MD trajectories, and the correlation maps. The following criteria were used.

The conformational ranking criterion is based on a comparison of the conformational space of the ligand in the complex with the conformational space of the free ligand. The best fit was obtained for the site **I**. The site **II** is characterized by a more labile intramolecular hydrogen bond in the ligand; however, its conformation is close to that corresponding to the global energy minimum. The sites **III** and **IV** are characterized by non-optimal dihedral angles near the carboline moiety.

The ranking criterion based on the visual analysis of the trajectory includes an investigation of the interactions between the ligand and particular amino acid residues or important sites of the protein as well as identification of the specific features of enzyme conformations that can help to explain the mechanism of non-competitive inhibition and complex stability. According to this criterion, the interaction of manzamine with the site **II** of GSK-3 seems to be optimal. This site is characterized by stable ligand orientation in the structurally important region of the kinase molecule and by structural rearrangements in the priming phosphate binding site. The site **I** is also characterized by similar structural changes; however, the ligand is located in the axin binding site, while binding in this site does not provide a complete explanation for the mechanism of non-competitive inhibition because the GSK-3β—axin complex is catalytically active unlike the GSK-3β—FRAT complex.[16] The advantage of the site **IV** over the site **III** consists in a longer stability period of the system.

Eventually, analysis of the correlation maps is based on their differences from the map for the *apo*-form of GSK-3β and on noticeable unique features that can be related to the visual analysis of trajectories. They are most pronounced in the map for the site **II**, whereas in the map for the site **III** they are least pronounced. By and large, the results of map ranking correspond to those of visual ranking.

Based on the aforesaid, one can suggest that the site **II** is the most probable ligand binding site because it is marked as optimal by the visual analysis and correlation maps criteria and as suboptimal by the conformational space criterion. This conclusion agrees with the results of a docking-based search for the binding site of GSK-3β to TDZD non-competitive inhibitors.[59] Interestingly, the results of ranking obtained using sophisticated computational methods generally agree with those of thorough visual analysis of MD trajectories. The correlation map approach is useful for solving the ambiguities of the visual analysis because it allows one to monitor structural rearrangements or changes in the structural mobility in the visual analysis of MD trajectories.

Thus, in the present work we have studied the possible modes of interaction of GSK-3β with non-competitive inhibitor manzamine A. Four potential sites of the kinase—ligand interaction were revealed and analyzed. The cavity between the glycine-rich loop, the loop C, and the activation loop is the most probable site of interaction. Representative snapshots of the corresponding MD trajectory can be used for the structure-based design of novel non-competitive GSK-3 inhibitors.

The authors express their gratitude to the Research Computing Center at the M. V. Lomonosov Moscow State University for providing the computing time and to Prof. D. A. Case for kindly providing us with an Academic License for the AMBER 10 software.

This work was financially supported by the Ministry of Education and Science of the Russian Federation (Federal Target Program "Scientific Research and Pedagogical Staff of Innovative Russia" P714) and the Russian Foundation for Basic Research (project No. 08-03-00783a).

References

1. N. Embi, D. B. Rylatt, P. Cohen, *Eur. J. Biochem.*, 1980, **107**, 519.
2. M. P. Mazanetz, P. M. Fischer, *Nat. Rev. Drug Discovery*, 2007, **6**, 464.
3. C. J. Phiel, C. A. Wilson, V. M.-Y. Lee, P. S. Klein, *Nature*, 2003, **423**, 435.
4. M. van Noort, J. Meeldijk, R. van der Zee, O. Destree, H. Clevers, *J. Biol. Chem.,* 2002, **277**, 17901.
5. B. W. Doble, J. R. Woodgett, *J. Cell Sci.*, 2003, **116**, 1175.
6. E. Droucheau, A. Primot, V. Thomas, D. Mattei, M. Knockaert, C. Richardson, P. Sallicandro, P. Alano, A. Jafarshad, B. Baratte, C. Kunick, D. Parzy, L. Pearl, C. Doerig, L. Meijer, *Biochim. Biophys. Acta*, 2004, **1607**, 181.
7. K. K. Ojo, J. R. Gillespie, A. J. Riechers, A. J. Napuli, C. L. M. J. Verlinde, F. S. Buckner, M. H. Gelb, M. M. Domostoj, S. J. Wells, A. Scheer, T. N. C. Wells, W. C. Van Voorhis, *Antimicrob. Agents Chemother.*, 2008, **52**, 3710.
8. J. R. Woodgett, *EMBO J.*, 1990, **9**, 2431.
9. K.-F. Lau, C. C. J. Miller, B. H. Anderton, P.-C. Shaw, *J. Peptide Res.*, 1999, **54**, 85.
10. S. Kaku, S. Chaki, M. Muramatsu, *Curr. Signal Transduction Ther.*, 2008, **3**, 195.
11. A. Takashima, M. Murayama, O. Murayama, T. Kohno, T. Honda, K. Yasutake, N. Nihonmatsu, M. Mercken, H. Yamaguchi, S. Sugiharai, B. Wolozin, *Proc. Natl. Acad. Sci. USA*, 1998, **95**, 9637.
12. S. Patel, J. Woodgett, *Cancer Cell*, 2008, **14**, 351.
13. C. J. Fiol, A. M. Mahrenholz, Y. Wang, R. W. Roeske, P. J. Roach, *J. Biol. Chem.*, 1987, **262**, 14042.
14. J.-H. Cho, G. V. W. Johnson, *J. Biol. Chem.*, 2003, **278**, 187.
15. S. Frame, P. Cohen, *Biochem. J.*, 2001, **359**, 1.

16. B. Bax, P. S. Carter, C. Lewis, A. R. Guy, A. Bridges, R. Tanner, G. Pettman, C. Mannix, A. A. Culbert, M. J. B. Brown, D. G. Smith, A. D. Reith, *Structure*, 2001, **9**, 1143.
17. D. A. E. Cross, D. R. Alessi, P. Cohen, M. Andjelkovich, B. A. Hemmings, *Nature*, 1995, **378**, 785.
18. H. M. Berman, J. Westbrook, Z. Feng, G. Gilliland, T. N. Bhat, H. Weissig, I. N. Shindyalov, P. E. Bourne, *Nucleic Acids Res.*, 2000, **28**, 235.
19. R. S. Jope, C. J. Yuskaitis, E. Beurel, *Neurochem. Res.*, 2007, **32**, 577.
20. S. H. Obligado, O. Ibraghimov-Beskrovnaya, A. Zuk, L. Meijer, P. J. Nelson, *Kidney Int.*, 2008, **73**, 684.
21. L. Rinnab, S. V. Schütz, J. Diesch, E. Schmid, R. Küfer, R. E. Hautmann, K.-D. Spindler, M. V. Cronauer, *Neoplasia*, 2008, **10**, 624.
22. Z. Wang, K. S. Smith, M. Murphy, O. Piloto, T. C. P. Somervaille, M. L. Cleary, *Nature*, 2008, **455**, 1205.
23. M. Medina, A. Castro, *Curr. Opin. Drug Discovery Dev.*, 2008, **11**, 533.
24. A. Martinez, M. Alonso, A. Castro, C. Pérez, F. J. Moreno, *J. Med. Chem.*, 2002, **45**, 1292.
25. A. Castro, A. Encinas, C. Gil, S. Bräse, W. Porcal, C. Pérez, F. J. Moreno, A. Martínez, *Bioorg. Med. Chem.*, 2008, **16**, 495.
26. K. V. Rao, M. S. Donia, J. Peng, E. Garcia-Palomero, D. Alonso, A. Martinez, M. Medina, S. G. Franzblau, B. L. Tekwani, S. I. Khan, S. Wahyuono, K. L. Willett, M. T. Hamann, *J. Nat. Prod.*, 2006, **69**, 1034.
27. M. Hamann, D. Alonso, E. Martín-Aparicio, A. Fuertes, M. J. Pérez-Puerto, A. Castro, S. Morales, M. L. Navarro, M. del Monte-Millán, M. Medina, H. Pennaka, A. Balaiah, J. Peng, J. Cook, S. Wahyuono, A. Martínez, *J. Nat. Prod.*, 2007, **70**, 1397.
28. M. A. Ibrahim, A. G. Shilabin, S. Prasanna, M. Jacob, S. I. Khan, R. J. Doerksen, M. T. Hamann, *Bioorg. Med. Chem.*, 2008, **16**, 6702.
29. M. S. Laport, O. C. S. Santos, G. Muricy, *Curr. Pharm. Biotechnol.*, 2009, **10**, 86.
30. R. Sakai, T. Higa, C. W. Jefford, G. Bernardinelli, *J. Am. Chem. Soc.*, 1986, **108**, 6404.
31. M. Tsuda, J. Kobayashi, *Heterocycles*, 1997, **46**, 765.
32. M. Yousaf, N. L. Hammond, J. Peng, S. Wahyuono, K. A. McIntosh, W. N. Charman, A. M. S. Mayer, M. T. Hamann, *J. Med. Chem.*, 2004, **47**, 3512.
33. G. M. Morris, D. S. Goodsell, R. S. Halliday, R. Huey, W. E. Hart, R. K. Belew, A. J. Olson, *J. Comput. Chem.*, 1998, **19**, 1639.
34. R. Huey, G. M. Morris, A. J. Olson, D. S. Goodsell, *J. Comput. Chem.*, 2007, **28**, 1145.
35. *SYBYL 8.0*, Tripos Inc., St. Louis (MO), USA.
36. M. F. Sanner, *J. Mol. Graphics Modell.*, 1999, **17**, 57.
37. J. Gasteiger, M. Marsili, *Tetrahedron*, 1980, **36**, 3219.
38. R. D. Clark, A. Strizhev, J. M. Leonard, J. F. Blake, J. B. Matthew, *J. Mol. Graphics Modell.*, 2002, **20**, 281.
39. G. Jones, P. Willett, R. Glen, A. R. Leach, R. Taylor, *J. Mol. Biol.*, 1997, **267**, 727.
40. I. D. Kuntz, J. M. Blaney, S. J. Oatley, R. Langridge, T. E. Ferrin, *J. Mol. Biol.*, 1982, **161**, 269.
41. I. Muegge, Y. C. Martin, *J. Med. Chem.*, 1999, **42**, 791.
42. M. D. Eldridge, C. W. Murray, T. R. Auton, G. V. Paolini, R. P. Mee, *J. Comput.-Aided Mol. Des.*, 1997, **11**, 425.
43. D. A. Case, T. A. Darden, T. E. Cheatham III, C. L. Simmerling, J. Wang, R. E. Duke, R. Luo, M. Crowley, R. C. Walker, W. Zhang, K. M. Merz, B. Wang, S. Hayik, A. Roitberg, G. Seabra, I. Kolossváry, K. F.Wong, F. Paesani, J. Vanicek, X. Wu, S. R. Brozell, T. Steinbrecher, H. Gohlke, L. Yang, C. Tan, J. Mongan, V. Hornak, G. Cui, D. H. Mathews, M. G. Seetin, C. Sagui, V. Babin, P. A. Kollman, *AMBER 10*, University of California, San Francisco (CA), 2008.
44. V. Hornak, R. Abel, A. Okur, B. Strockbine, A. Roitberg, C. Simmerling, *Proteins: Struct., Funct., Bioinf.*, 2006, **65**, 712.
45. J. Wang, R. M. Wolf, J. W. Caldwell, P. A. Kollman, D. A. Case, *J. Comput. Chem.*, 2004, **25**, 1157.
46. A. Jakalian, D. B. Jack, C. I. Bayly, *J. Comput. Chem.*, 2002, **23**, 1623.
47. J. Wang, W. Wang, P. A. Kollman, D. A. Case, *J. Mol. Graphics Modell.*, 2006, **25**, 247.
48. J.-P. Ryckaert, G. Ciccotti, H. J. C. Berendsen, *J. Comput. Phys.*, 1977, **23**, 327.
49. W. L. Jorgensen, J. Chandrasekhar, J. D. Madura, R. W. Impey, M. L. Klein, *J. Chem. Phys.*, 1983, **79**, 926.
50. W. Humphrey, A. Dalke, K. Schulten, *J. Mol. Graphics*, 1996, **14**, 33.
51. S. Gerlach, *LabPlot: Data Analysis and Visualisation*, http://labplot.sourceforge.net, 2009.
52. P. A. Kollman, I. Massova, C. Reyes, B. Kuhn, S. Huo, L. Chong, M. Lee, T. Lee, Y. Duan, W. Wang, O. Donini, P. Cieplak, J. Srinivasan, D. A. Case, T. E. Cheatham, *Acc. Chem. Res.*, 2000, **33**, 889.
53. R. Luo, L. David, M. K. Gilson, *J. Comput. Chem.*, 2002, **23**, 1244.
54. V. Tsui, D. A. Case, *Biopolymers*, 2000, **56**, 275.
55. J. Srinivasan, T. E. Cheatham III, P. Cieplak, P. A. Kollman, D. A. Case, *J. Am. Chem. Soc.*, 1998, **120**, 9401.
56. M. L. Connolly, *Science*, 1983, **221**, 709.
57. R. Dajani, E. Fraser, S. M. Roe, M. Yeo, V. M. Good, V. Thompson, T. C. Dale, L. H. Pearl, *EMBO J.*, 2003, **22**, 494.
58. N. Zhang, Y. Jiang, J. Zou, Q. Yu, W. Zhao, *Proteins*, 2009, **75**, 671.
59. A. Martinez, M. Alonso, A. Castro, I. Dorronsoro, J. L. Gelpí, F. J. Luque, C. Pérez, F. J. Moreno, *J. Med. Chem.*, 2005, **48**, 7103.
60. A. Converso, T. Hartingh, R. M. Garbaccio, E. Tasber, K. Rickert, M. E. Fraley, Y. Yan, C. Kreatsoulas, S. Stirdivant, B. Drakas, E. S. Walsh, K. Hamilton, C. A. Buser, X. Mao, M. T. Abrams, S. C. Beck, W. Tao, R. Lobell, L. Sepp-Lorenzino, J. Zugay-Murphy, V. Sardana, S. K. Munshi, S. M. Jezequel-Sur, P. D. Zuck, G. D. Hartman, *Bioorg. Med. Chem. Lett.*, 2009, **19**, 1240.
61. R. Ilouz, S. Pietrokovski, M. Eisenstein, H. Eldar-Finkelman, *J. Mol. Biol.*, 2008, **383**, 999.
62. Y. Cheng, Y. Zhang, J. A. McCammon, *Protein Sci.*, 2006, **15**, 672.

Received October 13, 2009;
in revised form January 25, 2010